Published in final edited form as:
Ultrasound Med Biol. 2011 October ; 37(10): 1734–1742. doi:10.1016/j.ultrasmedbio.2011.06.010.

COMPARISON OF SCANNING ACOUSTIC MICROSCOPY AND HISTOLOGY IMAGES IN CHARACTERIZING SURFACE IRREGULARITIES AMONG ENGINEERED HUMAN ORAL MUCOSAL TISSUES

Frank Winterroth[1,*], **Kyle W. Hollman**[1,4], **Shiuhyang Kuo**[2], **Kenji Izumi**[2,5], **Stephen E. Feinberg**[1,2], **Scott J. Hollister**[1], and **J. Brian Fowlkes**[1,3]

[1]Dept. of Biomedical Engineering, University of Michigan, Ann Arbor, MI, USA

[2]Dept. of Oral and Maxillofacial Surgery, University of Michigan, Ann Arbor, MI, USA

[3]Dept. of Radiology, University of Michigan, Ann Arbor, MI, USA

[4]Soundsight Research, Livonia, MI., USA

Abstract

Acoustic microscopy was used to monitor an *ex vivo* produced oral mucosal equivalent (EVPOME) developed on acellular cadaveric dermis (AlloDerm®). As seeded cells adhered and grew, they filled in and smoothed out the surface irregularities, followed by the production of a keratinized protective outermost layer. If non-invasive *in vitro* ultrasonic monitoring of these cellular changes could be developed, then tissue cultivation could be adjusted in-process to account for biological variations in the development of these stratified cell layers. Cultured keratinocytes (from freshly obtained oral mucosa) were harvested and seeded onto AlloDerm® coated with human type IV collagen and cultured 11 days. EVPOMEs were imaged on the 11th day post-seeding using a scanning acoustic microscope (SAM) which consists of a single-element transducer: 61 MHz center frequency, 32 MHz bandwidth, 1.52 f#. The specimen surface was determined by thresholding the magnitude of the signal at the first axial incidence of a value safely above noise: 20–40 dB above the signal for the water and 2-dimensional ultrasonic images were created using confocal image reconstruction. A known area from each micrograph was divided into 12–40 even segments and examined for surface irregularities. These irregularities were quantified and one-way ANOVA and linear regression analysis were performed to correlate the surface profiles for both the AlloDerm® and EVPOME specimens imaged by SAM. Histology micrographs of the AlloDerm® and EVPOME specimens were also prepared and examined for surface irregularities. Unseeded AlloDerm® averaged 7–9 surface changes per 400μm. The number of changes in surface irregularities decreased to 2–3 per 400μm on the mature EVPOMEs. The numbers of surface irregularities between the unseeded AlloDerm® versus developing EVPOME are similar for both histology and SAM 2D B-scan images. For the EVPOME 2D B-scan micrographs produced by SAM, the decrease in surface irregularities is indicative of the

[*]Corresponding Author, Address: Department of Biomedical Engineering, University of Michigan, 1101 Beal Ave., Lurie BME Bldg., No. 2122, Ann Arbor, MI. 48109, fwinterr@umich.edu.
[5]Current Address: Department of Oral Anatomy, Course for Oral Life Science, Niigata University Postgraduate School of Medical and Dental Sciences, Japan.

stratified epithelium formed by seeded oral keratinocytes; verified in the histology images between the AlloDerm® and EVPOME. A near 1:1 linear correlation shows the similarities between the two imaging modalities. SAM demonstrates its ability to discern the cell development and differentiation occurring on the EVPOME devices. Unlike histology, SAM measurements are non-invasive and can be used to monitor tissue graft development without damaging any cells/tissues.

Keywords

Acoustics; backscatter; echogenicity; AlloDerm®; EVPOME

INTRODUCTION AND LITERATURE

Apoptosis (programmed cell death) and necrosis (cell death as a result of injury, disease, or other pathologic state) play critical roles in physiologic processes. Ultrasound in the frequency range of 20–100 MHz has been shown to detect changes in cells and tissues undergoing apoptosis [Czarnota et. al. 1997, Kolios et. al. 2002, Taggart et. al. 2007]. However, the changes in backscatter ultrasound intensity are not fully understood and in the case of epithelial cells undergoing differentiation, apoptosis, and finally keratinization, not yet examined. Keratinized cells of the oral mucosa are morphologically and physiologically similar to skin and derived from the same ectodermal tissues during embryologic development [Alur et. al. 2001, De Mare et. al. 1990, Hoogstraate et. al. 1998]. The mechanical properties of both these tissues have yet to be tested and compared, neither has there been any comparisons with other similar ectoderm-derived soft tissues such as the ureter and vaginal mucosal tissues.

Our overall objectives are testing engineered tissues *in vitro* - specifically an *ex vivo* produced oral mucosal equivalent (EVPOME), and for assessing tissue performance after their grafting, *in situ*. EVPOME has been successfully developed and applied to patients in clinical studies [Izumi et. al. 2004]. This can be performed using non-invasive and non-destructive testing procedures. When studying EVPOME, we first analyze the tissue's structure as compared to that of natural mucosa; this is followed by testing to compare nonlinear mechanical function. The comparisons of EVPOME's similarities to natural mucosal tissues are performed using methods which do not affect the physical compositions of any tissues; this more accurately represents how these tissues appear *in vitro* or *in vivo*.

Background on the Oral Mucosal Epidermis and Keratinization

The oral mucosal epidermis is composed of a keratinized stratified squamous epithelium. The outermost layer is always composed of non-living, highly keratinized (cornified) cells that function to reduce water loss [Warner et. al. 1988]. After keratinocytes leave the germinal layer, they undergo a specialized form of cell death known as anoikis. Anoikis is initiated when cells detach from their surrounding environment and lose communication with it [Tortora et. al. 1993]. In keratinocytes, this programmed cell death includes the production of keratin filaments within the cell body while other sub-cellular products and organelles undergo attrition [Broekaert et. al. 1988, Holland et. al. 1997, Tu et. al. 1993]. Figure 1 provides an illustration of the oral mucosa, showing the principal cell layers above the basal lamina: stratum basale, stratum spinosum, stratum granulosum, and stratum corneum - and the accumulation of keratin. Figure 2a shows a histology micrograph of healthy oral mucosa, showing the features and functions of the aforementioned cell layers. Cells on the basal layer are more cuboidal in shape and mitotic. As these cells migrate toward the surface layer, they undergo differentiation, losing their water content, becoming more squamous in appearance, and accumulating keratin. When they reach the surface of the

mucosal tissue, these keratinocytes have undergone anoikis and are more fully integrated into a uniform keratinized layer.

Background on EVPOME

The development and use of EVPOME has demonstrated its clinical efficacy in intra-oral surgical grafts [Hotta et. al. 2007, Izumi et. al. 2003, Izumi et. al. 2004]. In addition, oral mucosa tissues have been clinically reported to be suitable for transplantation to treat vaginal agenesis [Lin et.al. 2003]. The oral mucosa's histology resembles that of skin: as new cells are formed on the basal lamina, the more matured cells migrate upward, undergoing apoptosis and keratinization as they migrate [Izumi et. al. 2004]; this same process occurs in the EVPOME tissues. Figure 2b provides a histology micrograph of EVPOME, comparing it with the aforementioned histology image of natural oral mucosa tissue. In both cases, there is a basal layer of mitotic and differentiating cells, followed by post-mitotic, differentiated cell layers, then an uppermost keratinized layer. What is still unknown is EVPOME's effectiveness as a substitute tissue replacement for other soft tissues such as dermal, vaginal, or urethral; EVPOME's elastic properties have not been studied nor compared to other natural soft tissues of the human body. Although the oral mucosa's histology resembles that of human epidermis and both tissue types are derived from ectodermal tissues, similarities in their physical properties have yet to be compared.

We had earlier compared EVPOME's morphology to a commercially available acellular cadaver epidermis (AlloDerm®) and natural oral mucosa [Izumi et. al. 2003, Winterroth et. al. 2009b]. AlloDerm® comes from cadaveric tissue: technicians remove a thin layer of skin and use antibiotics and other substances to remove the cells and donor DNA that may cause rejection. We examined and compared the surface characteristics of both unseeded AlloDerm® and mature EVPOME (11 days post-seeding) using scanning acoustic microscopy (SAM) - also called ultrasound biomicroscopy. Comparing radiofrequency (RF) backscatter at different stages of growth and development of the oral mucosal tissues has led to a better understanding of their physical properties [Srivastava 2007]. Our eventual goal is applying SAM to examine the principal cellular constituents within mature EVPOME and correlate how they individually or collectively contribute to the physical characteristics of the tissue specimen.

Although there are different biological tests to determine if cells undergo apoptosis or necrosis [Norleén et. al. 2004, Vermes et. al. 1995], there is no method to noninvasively test cell death in tissues or organs. Further, there are no studies which microscopically record the maturation and development of any cells and tissues, either *in vitro* or *in vivo.*

Background on SAM

Acoustic microscopy has been used for decades, mostly to non-invasively assess the structures and properties of engineered materials [Quate 1976]. It is just in the last several years that such technology has been applied to examine biological materials such as cells and tissues also. SAM has been proven an effective tool to study both the morphology and non-linear elastic characteristics of natural and engineered oral mucosal tissues [Cohn et.al. 1997a, Cohn et.al. 1997b]. The advantages of using SAM over conventional optical and electron microscopy include being able to image the cells and tissues without doing any preparations which could potentially kill or alter the tissues; this provides a more accurate representation of the tissues' natural properties. It will also provide evidence as to the degree of differentiation which the cells are undergoing without chemically affecting its properties [Dill-Müller et. al. 2007, Kolios et. al. 2003, Saijo et. al. 2004]. The reflectivity off of the tissue surfaces will provide the degree of surface roughness: as the EVPOME's cells undergo division, space-filling, and keratinization on the surface, there is an increase in the

brightness seen in the SAM 2D B-Scans of the EVPOME. The transducer's parameters are: 15 μm scanning step size in both the transverse and horizontal directions; a lateral resolution (R_{lat}) of 37μm; an axial resolution (R_{ax}) of 24μm; a depth of field (DOF) of 223μm; the f-number is 1.5. Z-axis was sampled at 300 mega samples/second. Axial resolution is the resolution in the direction of propagation and is determined by the length of the ultrasound pulse propagating in the tissue; lateral resolution is the resolution orthogonal to the propagation direction of the ultrasound wave. Table 1 provides further details of the SAM's operating mechanisms, including axial and lateral resolutions, DOF, and acoustic impedance.

Previously, we used SAM to compare any changes in the RF data to the EVPOME and natural human oral mucosal cells in general undergoing differentiation, apoptosis, and keratinization [Winterroth et. al. 2009b, Zuber et. al. 1999]. The spectral analysis results from SAM can be compared to histological images of the EVPOME tissues at different stages of growth and development. By correlating changes in the RF data to the EVPOME (and mucosal cells in general) undergoing differentiation, apoptosis, and keratinization, we can better understand the physiological processes of these cells as they evolve and proliferate along the prepared AlloDerm® surface.

For this study, we examined, compared, and quantified surface irregularities in the apical morphologies of AlloDerm® and mature EVPOME using SAM and standard brightfield microscopy. By first comparing the morphologies of the oral mucosal tissues – both natural and engineered, we can establish a better understanding of the physical characteristics when it comes to testing for similarities in the tissues' physical properties. We can then quantify the cellular constituents among each of the tissue types and correlate how each contributes to the physical behavior of their respective tissues. Correlating the changes in integrated backscatter to the differentiation of cells as they migrate and undergo apoptosis could lead to better methods to examine the stages of cellular differentiation.

MATERIALS AND METHODS

Tissue Preparation –EVPOME

The protocol for harvesting human oral mucosal tissue was approved by a University of Michigan Internal Review Board. All individuals signed informed consent before the tissue samples were procured. A keratinized oral mucosa sample was taken from an out-patient at the University of Michigan Oral and Maxillofacial Surgery Clinic. The methods for preparation have been described in greater detail previously [Izumi et. al. 2003, Izumi et. al. 2004]. Briefly, oral mucosa keratinocytes were enzymatically dissociated from the tissue sample, and a primary cell culture was established and propagated in a chemically-defined, serum- and xenogeneic products-free culture medium, with a calcium concentration of 0.06 mM. The AlloDerm® was soaked in 5 μg/cm^2 human type IV collagen overnight prior to seeding cells to assist the adherence of cells, then approximately 1.5×10^5 cells/cm^2 of oral keratinocytes were seeded onto the type IV collagen pre-soaked AlloDerm®. The composites of the keratinocytes and the AlloDerm® were then cultured, in the submerged condition, for 4 days with a calcium concentration of 1.2mM to form a continuous epithelial monolayer. After 4 days, the equivalents were raised to an air-liquid interface to encourage epithelial stratification and cultured for up to 10 days, resulting in a fully-differentiated, well-stratified epithelial layer on the AlloDerm®. At Day 11 post-seeding, EVPOME samples were collected for SAM imaging.

SAM Apparatus and Imaging

Details of the scanning and ultrasound system are similar to those described elsewhere [Cohn et. al. 1997a, Cohn et. al. 1997b, Hollman et. al. 2002]. AlloDerm®, EVPOME, and natural mucosal tissue samples were immersed in deionized water and imaged with a single element fixed focus transducer, producing ultrasonic B-scans. The transducer has an approximate frequency of 61 MHz, the element is 3 mm in diameter and focused to a depth of 4.1 mm, giving an f-number of approximately 1.4. The transducer was fastened to an optical mount and the angular position was adjusted until the ultrasonic beam was normal to the deflecting plate. We scanned the surfaces of the AlloDerm® and EVPOME (at different days post-seeding) showing the acoustic signal between the interface of the sample and water on the sample's apical side. DC stepper motors accurately positioned the transducer above the specimen. B-scan images were obtained by stepping the transducer element laterally across the desired region. At each position, the transducer fired and an RF A-line was recorded. After repeated firings at one position, the transducer moved to the next position, where the image was constructed from A-lines acquired at all lateral positions. Because of low f-number, single element transducers have a short depth of field, a composite B-scan image was generated from multiple scans at different heights. The general SAM set up with the mounted tissue is illustrated in Figure 3. Differences in the acoustic patterns as they reflect off of the tissue and immersion tank boundaries (surface and base) include the phase shift in the sound waves when reflecting off the tissue as opposed to the base surface of the holder, the reflections off the surface and bottom of the tissue, and the sound speed through water and tissue [11, 24, 33]. The spacing was determined by the step sizes along each of the axes: 15 μm scanning step size in both the transverse and horizontal directions (Y-axis and X-axis, respectively); a lateral resolution (R_{lat}) of 37μm; an axial resolution (R_{ax}) of 24μm; a depth of field of 223μm. Z-axis was sampled at 300 mega samples/second. R_{ax} is the resolution in the direction of propagation and is determined by the length of the ultrasound pulse propagating in the tissue; R_{lat} is the resolution orthogonal to the propagation direction of the ultrasound wave. The tissue surface was determined by thresholding the magnitude of the signal at the first axial incidence of a value safely above noise; approximately 30 dB above the signal of the water (Figure 4); this was kept consistent for all of the samples we scanned. Approximately 4–5 scans were performed for each of the AlloDerm® and EVPOME engineered tissue devices.

Histology

AlloDerm® and EVPOME (at different stages of growth following seeding of cells) were fixed with 10% formalin, embedded in paraffin, cut in 5 μm sections, and stained with hematoxylin and eosin. The specimens were then examined under a Nikon Ti-U inverted brightfield microscope (Nikon Optical, Tokyo, Japan).

Statistical Analyses

Both one-way ANOVA and student t-tests were performed on the stages of growth, differentiation, and eventual apoptosis of the cells.

In order to quantify the surface irregularities on both specimens imaged using both SAM and histological preparations, we fit the planar surface for all specimens and determined the number of variations in the tissues above and below the surface. A known area from each micrograph examined (300–1000μm × 100μm) was divided into 12–40 even segments: 4 rows, 4–10 columns; the total area for each divided segment would be 2610μm^2. Each segment was then examined for the number of irregularities between the foreground (tissue and device) and background (empty slide). The number of times the foreground (device) and background (empty slide) appears in each segment was then quantified for each row. The numbers for all rows were then added up, giving the total counts for the entire area. An

illustration of this segmentation method is seen in Figure 5. The surface irregularities were quantified and a linear regression analysis was performed to correlate the surface profiles for both the AlloDerm® and EVPOME categories imaged by both SAM and optical microscopy. To have an adequate number of images for quantifying surface irregularities, we categorized the total number of images examined into the following divisions along with the number of images micrographs examined:

SAM 2D B-Scans EVPOME: 8 SAM 2D B-Scans AlloDerm®: 8

Histology EVPOME: 7 Histology AlloDerm®: 7

RESULTS

Surface Morphologies in 2D B-Scans and Histology Micrographs

In the SAM 2D B-scan for the AlloDerm® device, the transducer is positioned at the top of the image, pointing downward. The top bright echo indicates the boundary between the coupling medium (water) and the apical surface of the AlloDerm®. Below this, the tissue device appears as uniform speckle; there is no second boundary between the tissue interface and the lower tissues. True surfaces from the specular reflections are rendered at the threshold value, not at the peak. The large bright spots indicate backscatter and are approximately 30μm in diameter. Based on this reflectivity (namely, the degree of the ultrasonic signal that it reflected back to the transducer; the greater the reflected signal from any given material will produce a brighter image in the B-Scan), there is a much brighter, more uniform surface layer in the SAM EVPOME images; in contrast, the AlloDerm® images do not display this bright surface layer (Figure 6).

The undulated surface of the AlloDerm® results in higher presence of grayscale within the surface (Figure 6a) as compared to the EVPOME image (Figure 6b). Based on this reflectivity, it is clear that there is a clear difference in the SAM images showing surface properties between the AlloDerm® and the EVPOME. Histology micrographs of these same tissues - AlloDerm® and EVPOME - validate this finding (Figure 7a and 7b).

Quantifying Surface Irregularities and Statistical Correlations

The correlations for the number of irregularities versus the unseeded AlloDerm® and development of the mature EVPOME (at 11 days post-seeding) are similar for both 2D SAM B-scan images and histology micrographs (Figure 8a and 8b, respectively). The unseeded AlloDerm® averaged 7–9 surface changes per 400μm; the number of changes decreases to 2–3 per 400μm for the EVPOME specimens.

The linear regression analyses comparing the AlloDerm® and EVPOME samples verifies this decrease between approximately 2.69 to 3.87 fold between the undulation counts for AlloDerm® and EVPOME when examining both SAM and histology (Figure 9a and 9b, respectively). The standard error of the mean (namely, the standard deviation divided over the mean number of surface irregularities) was incorporated into the linear regression; correlating the number of irregularities in the 2D B-scan SAM to those found in the histology images shows a mean correlation coefficient of 1.09. This establishes a near 1:1 correlation between the mean counts between both microscopy tools.

DISCUSSION

The 2D and 3D SAM scanned images of the mature EVPOME shows increased ultrasonic reflection on the surface; this is indicative of the keratinocytes' proliferation and space-filling properties, plus the keratin uniformity. Such uniformity results from the supe rficial

keratinized layer of stratified epithelium formed by seeded oral mucosa keratinocytes; the histology micrograph of the EVPOME's surface verify this uniformity (Figure 7b). The EVPOME's keratinized surface is set at the threshold of the acoustic signal; the images taken of this surface show a near seamless image of blue along the surface of the tissue – this is strongly evident of the space-filling characteristics of keratin and keratinocytes. The keratinocytes' adaptability to grow, proliferate, and differentiate on the AlloDerm® scaffold strongly supports EVPOME's potential as an ideal graft material [Izumi et. al. 2003, Izumi et. al. 2007].

Testing for ANOVA within the group of engineered tissues shows differences between the scans within the experiment as a whole. The SAM images comparing the surfaces between the AlloDerm® and EVPOME show an average 2.69 to 3.87 fold decrease in the number of irregularities as the keratinocytes on the EVPOMEs' surfaces undergo maturation, proliferation, and keratinization. As the oral keratinocytes adhere and mature on the AlloDerm® surface, they proliferate and subsequently fill in the rough surface of the specimen. Further maturation of these cells eventually leads to their apoptosis and keratinization which occurs on the apex of the filled-in surface; this is evident by the bright reflectivity seen in the SAM B-Scans and the smooth layer visible in the histology micrographs (Figures 6 and 7, respectively). SAM demonstrates its ability to discern the differences in the surfaces between the two specimens. This further verifies acoustic microscopy as an effective imaging modality for cells and tissues and their subsequent evolution and differentiation.

A strong linear correlation is noticed when quantifying and comparing surface irregularities between the AlloDerm® and EVPOME micrographs from both SAM and histology (Figure 9). The high resolution in the 2D images produced and the accuracy in images between acoustic and optical microscopy demonstrate SAM as an excellent complement to imaging cells and tissues. SAM has the added advantage over histology imaging as there is no need to prepare the specimens in any manner prior to imaging.

We are currently using SAM to analyze both natural oral mucosa and EVPOME's potential as a surgical graft material; this includes applying ultrasonics to examine these same tissues' elastic properties. The buccal has been studied for its structure and efficacy in drug delivery [Alur et. al. 2001, Hoogstraate et. al. 1998], but its potential as a surrogate for soft tissue reconstruction is rather limited. Although the morphology of the EVPOME - in its early stages of development at least – shows great promise in its space-filling abilities, testing its functional similarities to natural tissues has yet to be performed. Further, both EVPOME and natural oral mucosal tissues must tested be *in situ* to get the best results for their long-term adaptability and durability as an aforementioned replacement tissue.

Ultrasonic B-scans (and their corresponding histology images) are not detecting seeded cells filling in the irregularities of the specimen until cells have sufficiently stratified and differentiated [Winterroth 2009a, Winterroth 2009b]. The more maturely differentiated tissues, present at day 11 showing brighter echogenicity and less surface variance are possibly due to cellular changes resulting from an increase in stratification – verified by the histology at these days. These initial results show that ultrasonic characterization may have the potential to monitor EVPOME development during its growth and differentiation. Because SAM requires no preparatory work on the specimens, we are currently producing a protocol to image a set of EVPOMEs under aseptic conditions to effectively monitor the kerotinocytes' growth and differentiation (from day 1 post – seeding up until they are fully mature) based on changes in their acoustic patterns and their 2D B-Scan images.

Acknowledgments

This work was supported through the National Institutes of Health (NIH) Regenerative Sciences Training Grant Number 5T90DK070071 and NIH Grant Numbers R21EY018727, R01 DE13417, and NIH center core (P30) grant, EY007003. National Institutes of Health, Bethesda, MD. 20892. We gratefully acknowledge the NIH Resource Center for Medical Ultrasonic Transducer Technology at the University of Southern California (Los Angeles, CA. 90089) for designing and building the high frequency transducer used in this study.

References

Alur, HH.; Johnson, TP.; Mitra, AK. Peptides and Proteins: Buccal Absorption. In: Swarbrick, J.; Boylan, JC., editors. Encyclopedia of Pharmaceutical Technology. Vol. 20. Marcel Dekker; 2001. p. 193-218.

Broekaert D, Van Oostveldt P. Nuclear Differentiation During Epidermal Keratinization. Arch Dermatol Res. 1988; 280:188–189.

Czarnota GJ, Kolios MC, Vaziri H, Benchimol S, Ottensmeyer FP, Sherar MD, Hunt JW. Ultrasonic Biomicroscopy of Viable, Dead, and Apoptotic Cells. Ultrasound in Med Biol. 1997; 23:961–965. [PubMed: 9301000]

Cohen RD, Mottley JG, Miller JG, Kurnik PB, Sobel BE. Detection of Ischemic Myocardium in Vivo Through the Chest Wall by Quantitative Ultrasonic Tissue Characterization. Amer J Cardiol. 1982; 61:838–843. [PubMed: 7124643]

Cohn NA, Emelianov SY, Lubinski MA, O'Donnell M. An Elasticity Microscope. Part I: Methods. IEEE Trans Ultrason Ferr Freq Ctrl. 1997; 44(6):1304–1319.

Cohn NA, Emelianov SY, O'Donnell M. An Elasticity Microscope. Part II: Experimental Results. IEEE Trans Ultrason Ferr Freq Ctrl. 1997; 44(6):1320–1331.

De Mare S, Van Erp PEJ, Ramaekrs FCS, Van De Kerkhof PCM. Flow Cytometric Quantification of Human Epidermal Cells Expressing Keratin 16 *In Vivo* After Standardized Trauma. Arch Derm Res. 1990; 282:126–130. [PubMed: 1693838]

Dill-Müller D, Maschke J. Ultrasonography in Dermatology. Journal der Deutschen Dermatologischen Gesellschaft. 2007; 5:689–707. [PubMed: 17659044]

Eccles SA, Massey A, Raynaud FI, Sharp SY, Box G, Valenti M, Patterson L, de Haven Brandon A, Gowan S, Boxall F, Aherne W, Rowlands M, Hayes A, Martins V, Urban F, Boxall K, Prodromou C, Pearl L, James K, Matthews TP, Cheung KM, Kalusa A, Jones K, McDonald E, Barril X, Brough PA, Cansfield JE, Dymock B, Drysdale MJ, Finch H, Howes R, Hubbard RE, Surgenor A, Webb P, Wood M, Wright L, Workman P. NVP-AUY922: A Novel Heat Shock Protein 90 Inhibitor Active Against Xenograft Tumor Growth, Angiogenesis, and Metastasis. Cancer Res. 2008; 68(8):2861–60. [PubMed: 18413754]

Holland MR, Hall CS, Lewis SH, Handley SM, Finch-Johnston AE, D'Sa AP, Perez JE, Miller JG. Comparison of Integrated Backscatter Values Obtained with Acoustic Densitometry with Values Derived from Spectral Analysis of Digitized Signals from a Clinical Imaging System. J Amer Soc Echocardio. 1997; 10(5):511–517.

Hollman KW, Emelianov SY, Neiss JH, Jotyan G, Spooner GJR, Juhasz T, Kurtz RM, O'Donnell M. Strain Imaging of Corneal Tissue With an Ultrasound Elasticity Microscope. Cornea. 2002; 21(1): 68–73. [PubMed: 11805511]

Hoogstraate JAJ, Wertz PW. Drug Delivery via the Buccal Mucosa. Pharm Sci Tech Tod. 1998; 1(7): 309–316.

Hotta T, Yokoo S, Terashi H, Komori T. Clinical and Histopathological Analysis of Healing Process of Intraoral Reconstruction with *Ex Vivo* Produced Oral Mucosa Equivalent. Kobe J Med Sci. 2007; 53(1):1–14. [PubMed: 17579297]

Izumi K, Feinberg SE, Iida A, Yoshizawa M. Intraoral Grafting of an *Ex Vivo* Produced Oral Mucosa Equivalent: A Preliminary Report. Int J Oral Maxillofac Surg. 2003; 32:188–197. [PubMed: 12729781]

Izumi K, Song J, Feinberg SE. Development of a Tissue-Engineered Human Oral Mucosa: From the Bench to the Bed Side. Cells Tissues Organs. 2004; 176:134–152. [PubMed: 14745242]

Izumi K, Tobita T, Feinberg SE. Isolation of Human Oral Keratinocyte Progenitor/Stem Cells. J Dent Res. 2007; 86(4):341–346. [PubMed: 17384029]

Kolios MC, Czarnota GJ, Lee M, Hunt JW, Sherar MD. Ultrasonic Spectral Parameter Characterization of Apoptosis. Ultrasound in Med Biol. 2002; 28(5):589–597. [PubMed: 12079696]

Kolios, MC.; Taggart, L.; Baddour, RE.; Foster, FS.; Hunt, JW.; Czarnota, GJ.; Sherar, MD. An Investigation of Backscatter Power Spectra from Cells, Cell Pellets, and Microspheres. IEEE Ultrasonics Symposium; 2003. p. 752-757.

Lin WC, Chang CYY, Shen YY, Tsai HD. Use of Autologous Buccal Mucosa for Vaginoplasty: A Study of Eight Cases. Human Reproduction. 2003; 18(3):604–607. [PubMed: 12615833]

Matsuyama H, St Goar FG, Tye TL, Oppenheim G, Schnittger I, Popp RL. Ultrasonic Tissue Characterization of Human Hypertrophied Hearts *In Vivo* with Cardiac Cycle-Dependent Variation in Integrated Backscatter. Circul. 1989; 80:925–934.

Norleén L, Al-Amoudiz A. Stratum Corneum Keratin Structure, Function, and Formation: The Cubic Rod-Packing and Membrane Templating Model. J Invest Dermatol. 2004; 123:715 –732. [PubMed: 15373777]

Quate, CF. Imaging Using Lenses. In: Wade, G., editor. Acoustic Imaging: Cameras, Microscopes, Phased Arrays, and Holographic Systems. NY: Plenium Press; 1976. p. 241-305.

Revell, J.; Mirmehdi, M.; McNally, D. Ultrasound Speckle Tracking for Strain Estimation. 2003. http://www.cs.bris.ac.uk/~revell

Saijo Y, Miyakawa T, Sasaki H, Tanaka M, Nitta S. Acoustic Properties of Aortic Aneurysm Obtained with Scanning Acoustic Microscopy. Ultrasonics. 2004; 42:695–698. [PubMed: 15047369]

Saijo Y, Tanaka M, Okawai H, Dunn F. The Ultrasonic Properties of Gastric Cancer Tissues Obtained with a Scanning Acoustic Microscope. Ultrasound in Med & Biol. 1991; 17(7):709–714. [PubMed: 1781074]

Somekh MG, Bertoni HL, Briggs GAD, Burton NJ. A Two-Dimensional Imaging Theory of Surface Discontinuities with the Scanning Acoustic Microscope. Proceedings of the Royal Society of London Series A, Mathematical and Physical Sciences. 1985; 401(1820):29–51.

Srivastava, R. Apoptosis, Cell Signaling, and Human Diseases: Molecular Mechanisms. NY: Humana Press; 2007. p. 157402 pages

Taggart LR, Baddour RE, Giles A, Czarnota GJ, Kolios MC. Ultrasonic Characterization of Whole Cells and Isolated Nuclei. Ultrasound in Med & Biol. 2007; 33(3):389–401. [PubMed: 17257739]

Tortora, GJ.; Grabowski, SR. Principles of Anatomy and Physiology. 7. HarperCollins College Publisher; New York: 1993.

Tu HP, Chen YT, Chiu HC, Chin Y-T, Huang S-M, Cheng L-C, Fu E, Chiang C-Y. Cyclosporine A Enhances Apoptosis in Gingival Keratinocytes of Rats and in OECM1 Cells via the Mitochondrial Pathway. J Periodontal Res. 2009; 44(6):767–775. [PubMed: 19602127]

Vermes I, Haanen C, Steffens-Nakken H, Reutellingsperger C. A Novel Assay for Apoptosis. Flow Cytometric Detection of Phosphatidylserine Expression on Early Apoptotic Cells Using Fluorescein Labelled Annexin V. J Immunol Methods. 1995; 184(1):39–51. [PubMed: 7622868]

Warner RR, Myers MC, Taylor DA. Electron Probe Analysis of Human Skin: Determination of the Water Concentration Profile. J of Invest Dermatol. 1988; 90:218–224. [PubMed: 3339263]

Winterroth, F.; Hollman, KW.; Izumi, K.; Feinberg, SE.; Fowlkes, JB.; Hollister, SJ. Examination and Comparisons of EVPOME/AlloDerm® Compositions with Natural Mucosal Tissues Using Scanning Acoustic Microscopy. Society for Biomaterials 2009 Annual Meeting and Exposition; 2009a.

Winterroth, F.; Fowlkes, JB.; Kuo, S.; Izumi, K.; Feinberg, SE.; Hollister, SJ.; Hollman, KW. High-Resolution Ultrasonic Monitoring of Cellular Differentiation in an *Ex Vivo* Produced Oral Mucosal Equivalent (EVPOME). Proc. IEEE Bioultrasonics Conference; 2009b.

Zuber M, Gerber K, Erne P. Myocardial Tissue Characterization in Heart Failure by Real-Time Integrated Backscatter. Eur J Ultrasound. 1999; 9:135–143. [PubMed: 10413749]

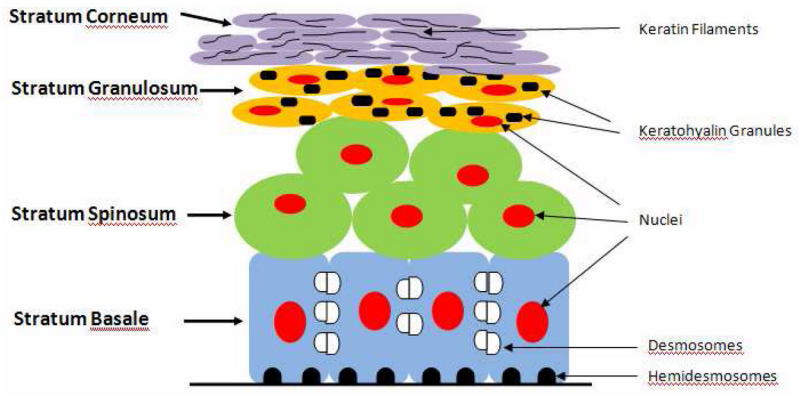

Figure 1.
Illustrative schematic of the oral mucosa showing the principal cells and structures which constitute the oral lining above the basal lamina. The cell layers near the basal side appear more cuboidal; as they migrate toward the apex, they become more squamous and undergo apoptosis and keratinization.

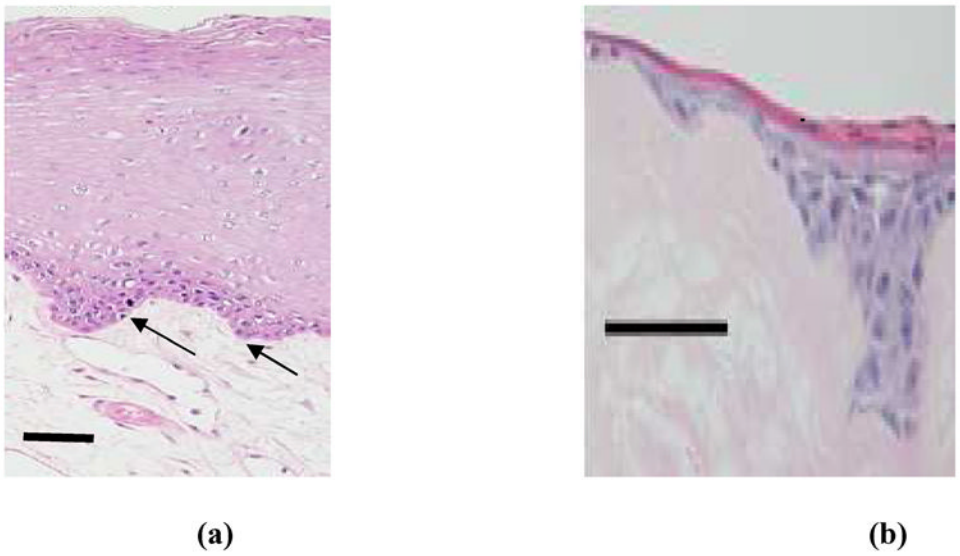

Figure 2.
Histology of natural oral mucosa tissue (a) and EVPOME device (b). In both cases, there is a basal layer of actively dividing and differentiating cells (arrows), followed by a uniformly keratinized surface (asterisk). Scale bars represent 100μm.

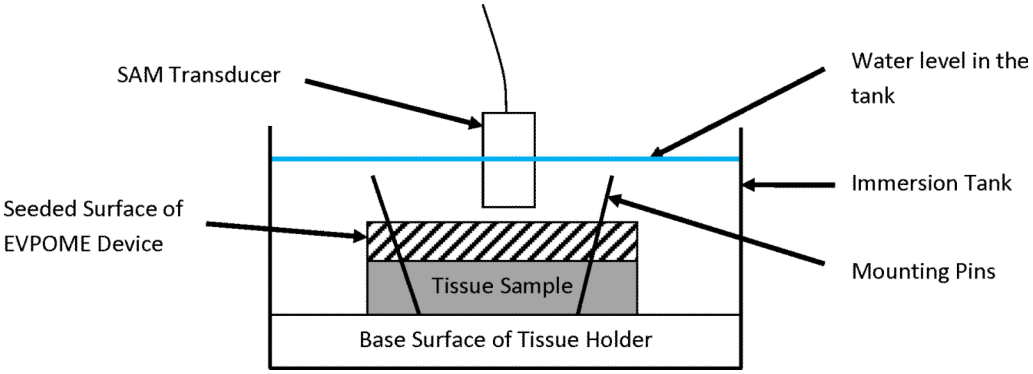

Figure 3.

Illustrative set-up of the SAM, showing principal features for the scan. The devices (AlloDerm® and EVPOME) are mounted on the tissue holder using either pins or adhesive. The devices are then immersed in degassed, deionized water with the scanning transducer placed directly over them. The focal length is then adjusted for each sample being scanned the surfaces of the AlloDerm® and EVPOME at different days post-seeding showing difference in the acoustic reflections off of the surface of the apical surfaces for each of the devices. Note: the sizes of the devices, tank, transducer, and other objects are not to scale.

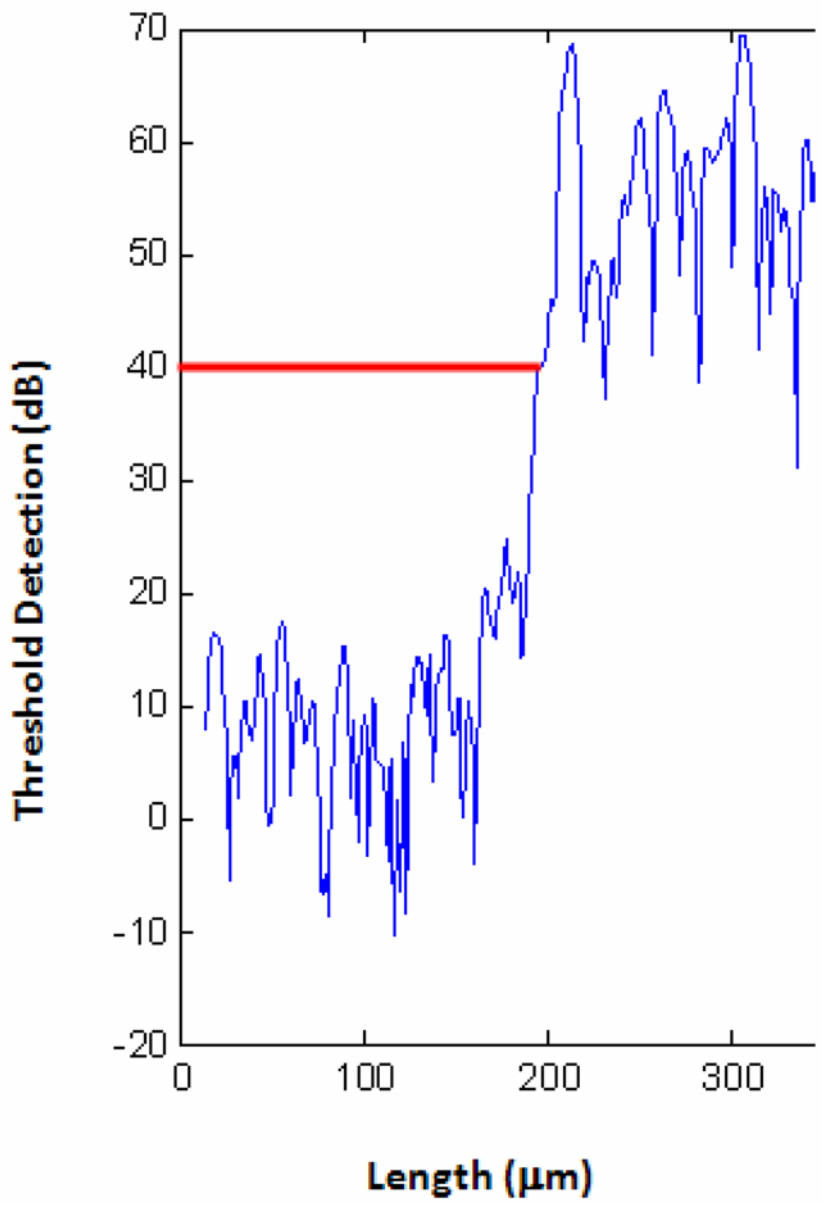

Figure 4.
Plot diagram of the SAM, showing the detection of the device surface (red line) after setting the threshold detection safely above the signal of the water.

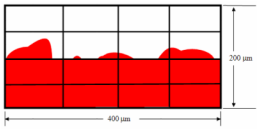

Figure 5.
Illustrative set-up used to quantify the surface irregularities for both the AlloDerm® and EVPOME images. A known area (80,000 μm^2) of each micrograph was divided into 16 even segments - 4 rows, 4 columns; each segment being 5000μm^2 in area. The number of times the foreground (device, shown in red) and background (empty slide, shown in white) appear in each segment were then quantified for each row. The numbers for all rows were then added up, giving the total counts for the entire area. Illustration is not to scale.

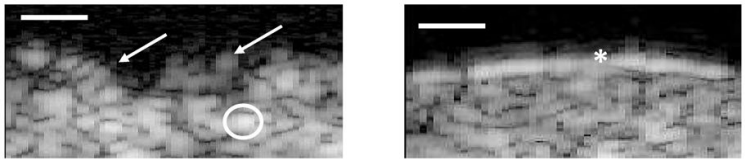

Figure 6.
SAM 2D B-Scan images of a typical unseeded AlloDerm® (a) and mature EVPOME (b). The high presence of grayscale on the AlloDerm® surface shows greater scatter off of the surface compared to the EVPOME indicative of the surface irregularities (arrows). The large bright spots indicate backscatter (circled). Note the bright band on the surface of the EVPOME, a characteristic of the higher reflectivity off of the surface resulting from the keratinized surface (asterisk). Scale Bars = 100μm.

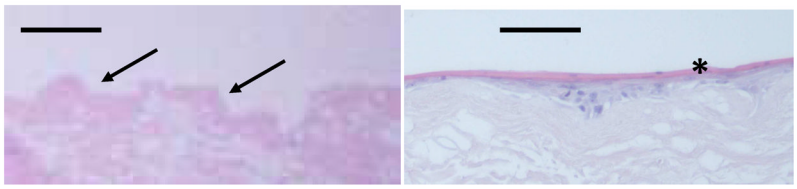

Figure 7.
Histology micrographs comparing a typical unseeded AlloDerm® (a) and mature EVPOME (b). Note the higher number of surface irregularities on the former (arrows); by contrast, the EVPOME has a smoother surface due to the presence of the cells and the keratin layer (asterisk). Scale Bars = 100μm.

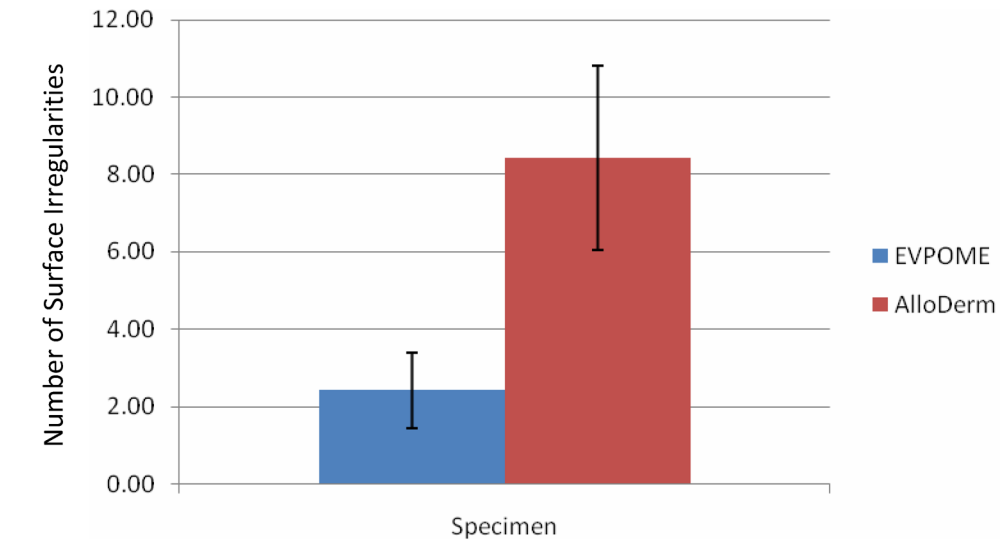

a

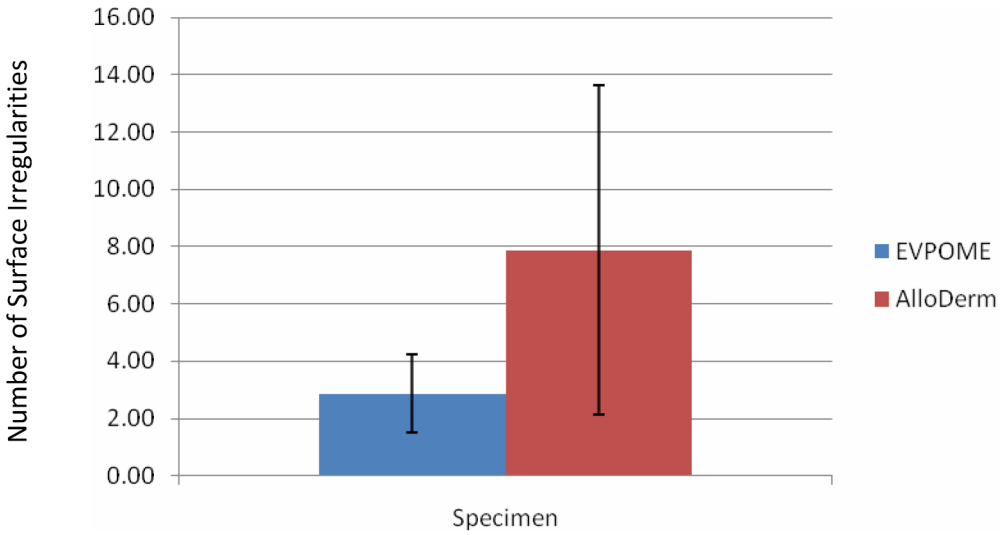

b

Figure 8.
SAM 2D B-Scan comparisons (a) and histology micrograph comparisons (b) between the average numbers of surface irregularities observed between mature EVPOME (11 days post-seeding) and unseeded AlloDerm®.

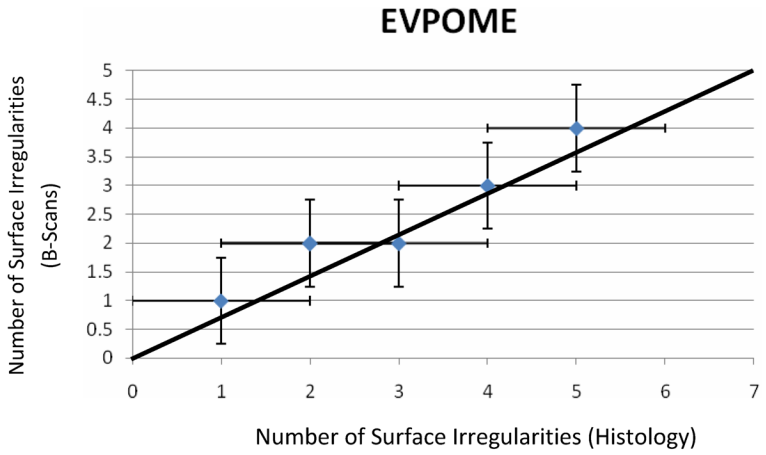

a

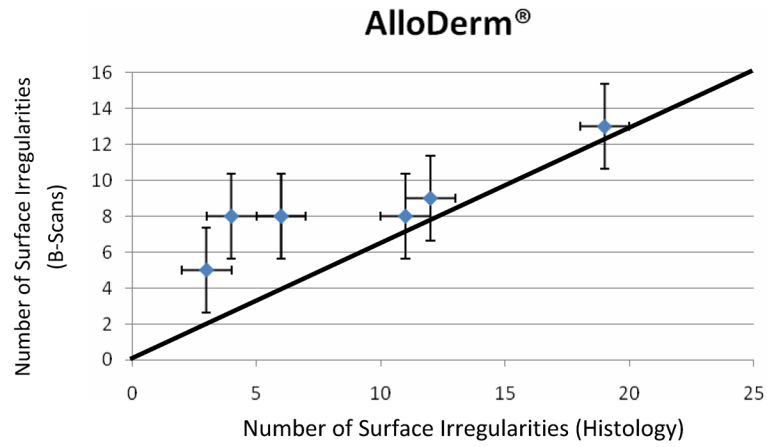

b

Figure 9.
Linear correlation showing the mature EVPOME (a) and AlloDerm® (b) surface irregularity counts observed between the SAM 2D B-Scans versus the histology micrographs.

Table 1

Compendium of the operating details for use in ultrasonic microscopy, including basic equations of the SAM operating principles: axial and lateral resolutions, DOF, and acoustic impedance.

Equation	Term	Application
1. $R_{ax}=\frac{c}{2\times BW}$	Axial Resolution	Resolution depends on the dimensions of the pressure pulse, which is related to the transducer bandwidth (BW) and system electronics, where *c* is the sound speed in the tissue and BW is 32MHz.
2. $R_{lat}=\lambda \times$ f-number	Lateral Resolution	Resolution at the focal point, where λ is the wavelength(25μm). Lateral resolution is the resolution orthogonal to the propagation direction of the ultrasound wave.
3. DOF=4(f-number)^2 λ	Depth of Field (DOF)	Due to a small f-number(which provides a tight beamwidth), the DOF is also limited.
4. Z= ρc	Acoustic Impedance	Impedance (Z) determines the amplitude of the reflected and transmitted waves at the fluid- interface. Complex scattering properties of tissues are due to acoustic impedance interfaces in microstructure of tissues. ρ is the material density.
5. R = |(Z2−Z1)/(Z2+Z1)|	Reflection Coefficient	Ratio of the impedance mismatch between the two materials – fluid and tissue specimen.